ACKNOWLEDGEMENTS

The authors would like to thank many members of the JET team and especially the Soft X-ray Group for their assistance. They would also like to thank J. Wesson and J. Hastie for useful discussions and J. Peters for helping with the analysis of the data.

REFERENCES

[1] LAZZARO, E., MANTICA, P., Experimental Identifications of Tokamak Equilibrium using Magnetic and Diagnostic Signals, Rep. JET-P (87) 58, JET Joint Undertaking, Abingdon, Oxfordshire (1987).
[2] O'ROURKE, J., BLUM, J., CORDEY, J.G., et al., in Controlled Fusion and Plasma Heating (Proc. 15th Eur. Conf. Dubrovnik, 1988), Vol. 12B, Part I, European Physical Society (1988) 155.
[3] GRANETZ, R.S., EDWARDS, A.W., GILL, R.D., WELLER, A., in Controlled Fusion and Plasma Physics (Proc. 14th Eur. Conf. Madrid, 1987), Vol. 11D, Part II, European Physical Society (1977) 1256.
[4] WELLER, A., CHEETHAM, A.D., EDWARDS, A.W., et al., Phys. Rev. Lett. **59** (1987) 2303.
[5] TFR Group, Nucl. Fusion **27** (1987) 1975.
[6] PARKS, P.B., TURNBULL, R.J., Phys. Fluids **21** (1978) 1735.
[7] HOULBERG, W.A., MILORA, S.L., ATTENBERGER, S.E., Nucl. Fusion **28** (1988) 595.
[8] KAUFMANN, M., Plasma Phys. Controll. Fusion **28** (1986) 1341.
[9] McNEIL, D.H., GREENE, G.J., SCHURESKO, D.D., Phys. Rev. Lett. **55** (1985) 1398.
[10] GILL, R.D., Nucl. Fusion **29** (1989) 397.
[11] PARKS, P.B., Nucl. Fusion **20** (1980) 311.
[12] KADOMTSEV, B.B., Sov. J. Plasma Phys. **1** (1975) 389.
[13] CAMPBELL, D.J., GILL, R.D., GOWERS, C.W., et al., Nucl. Fusion **26** (1986) 1085.
[14] EDWARDS, A.W., CAMPBELL, D., ENGELHARDT, W.W., et al., Phys. Rev. Lett. **57** (1986) 210.
[15] WESSON, J.A., KIRBY, P., NAVE, M.F., in Plasma Physics and Controlled Nuclear Fusion Research 1986 (Proc. 11th Int. Conf. Kyoto, 1986), Vol. 2, IAEA, Vienna (1987) 3.
[16] BUSSAC, M.N., LERBINGER, K., PELLAT, R., TAGGER, M., ibid., p. 17.
[17] HASTIE, R.J., HENDER, T.C., CARRERAS, B.A., CHARLTON, L.A., HOLMES, J.A., Phys. Fluids **30** (1987) 2870.
[18] GILL, R.D., CAMPBELL, D., DUPERREX, P.A., et al., in Controlled Fusion and Plasma Heating (Proc. 15th Eur. Conf. Dubrovnik, 1988), Vol. 12B, Part I, European Physical Society (1988) 350.

(Manuscript received 28 October 1988
Final manuscript received 13 February 1989)

PITCH ANGLE RESOLVED MEASUREMENTS OF ESCAPING CHARGED FUSION PRODUCTS IN TFTR

S.J. ZWEBEN (Princeton Plasma Physics Laboratory, Princeton University, Princeton, New Jersey, United States of America)

ABSTRACT. Measurements of the flux charged fusion products escaping from the TFTR plasma have been made with a new type of detector which can resolve the particle flux versus pitch angle, energy and time. The design of this detector is described, and results from the 1987 TFTR run are presented. These results are approximately consistent with predictions from a simple first-orbit particle loss model with respect to the pitch angle, energy, time and plasma current dependences of the signals.

1. INTRODUCTION

Tokamak ignition with D–T fuel depends upon alpha particle heating, which in turn depends upon good alpha particle confinement. Good alpha particle confinement (i.e. less than 10% alpha loss) is predicted by the classical single-particle model at plasma currents above 3 MA [1]. In this model the alpha losses to the wall are mainly due to the prompt first-orbit loss, while almost all alphas confined on their first orbit stay confined until they are thermalized after about one second.

However, if unexpected alpha particle losses are encountered, for example due to background plasma or alpha particle induced instabilities [1, 2], then ignition will be more difficult. Therefore, it seems worth while to use presently available alpha-like charged fusion products, i.e. the 1 MeV triton and the 3 MeV proton

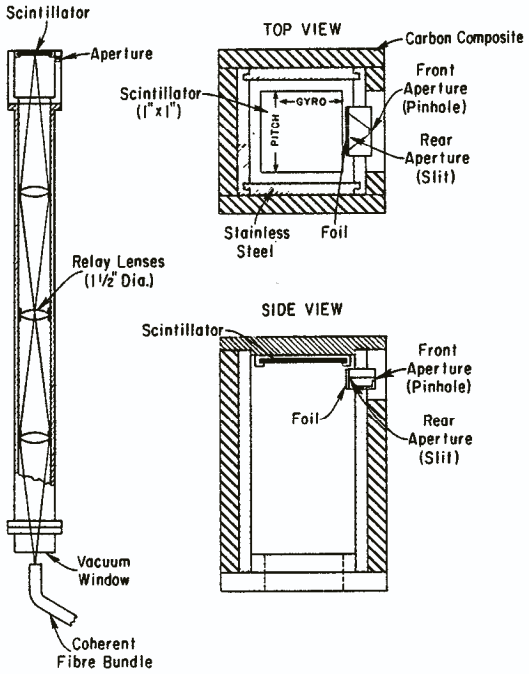

FIG. 1. Schematic views of the detector. The scintillator is mounted at the end of a probe inserted into the bottom of the TFTR vacuum vessel. The charged fusion products are dispersed according to pitch angle along one dimension of the scintillator and according to gyroradius (i.e. energy) along the other dimension (in orthogonal polar co-ordinates). The 2-D scintillator image is optically coupled to a video camera and a videocassette recorder.

from D–D reactions [3], to test the classical single-particle confinement model.

This letter describes the behaviour of the escaping D–D charged fusion products as measured during the 1987 operation of TFTR. These particles were detected just outside the plasma boundary with a new 2-D imaging detector system which can measure flux versus pitch angle, energy and time, as described in Section 2. The results obtained so far are approximately consistent with the predictions of a classical first-orbit loss model, as described in Section 3. The conclusions, including prospects for future measurements along these lines, are given in Section 4.

2. DETECTOR DESIGN

The present detector combines the features of two earlier designs. The geometry is similar to that used in an early PLT experiment [4] which measured D–^{3}He fusion products with a plastic track detector. That design had good pitch angle resolution and fair energy resolution, but no time resolution, since the plastic had to be removed and examined for individual particle tracks. This difficulty is avoided here by using instead of the plastic detector a ZnS scintillator screen which is optically coupled to a video camera for good time resolution. The ZnS scintillator itself was tested in a recent TFTR experiment [5] which measured D–D fusion products, but without pitch angle or energy resolution.

Schematic views of the present detector are shown in Fig. 1. The detection element itself is a 1 in × 1 in ZnS(Ag) scintillator screen mounted inside a light-tight stainless steel, carbon armoured box. This scintillator screen is oriented so that particles which pass through the front 'pinhole' and rear 'slit' apertures impact the 10–15 μm ZnS layer, which is supported by a 1 mm quartz substrate. The resulting 2-D image of the scintillation light (450–500 nm) is optically coupled through a relay lens system to a coherent fibre bundle for transmission to a video camera located in a shielded basement.

The pitch angle of the particles, χ (i.e. the angle of their gyromotion with respect to the toroidal field B_T), is determined by the angle between the front 'pinhole' and the impact position as measured along the 'pitch angle' co-ordinate of the scintillator (Fig. 2(a)). The geometrical pitch angle resolution of $\delta\chi \approx \pm 3°$ (FWHM) is determined by the width of the front aperture, W = 2 mm. The range of detected pitch angles, $\chi \approx 45$–$85°$, is determined by the scintillator size and by the orientation of the detector box. The box is aligned at $\approx 65°$ with respect to B_T to see the expected classical first-orbit losses, as described in Section 3.1.

The triton energy E is inferred through a measurement of its gyroradius, ρ (cm) = $4.5E^{1/2}$ (MeV) sin χ/B_T (50 kG), where B_T is the toroidal field (see Fig. 2(b)). The gyroradius of typically $\rho \approx 4$–5 cm is inferred from the particle impact position B through $B^2 = 2D\rho + A^2$. The geometrical energy resolution of about $\pm 50\%$ is determined by the finite height of the apertures, H = 1 mm (full height), which, in turn, is determined by the required detector sensitivity. Good energy resolution is considered of secondary importance here, since the Doppler width of $\pm 25\%$ for beam–target produced tritons is expected to dominate the energy spectrum.

The sensitivity of the detector is determined by the areas of the front and rear apertures. These areas are

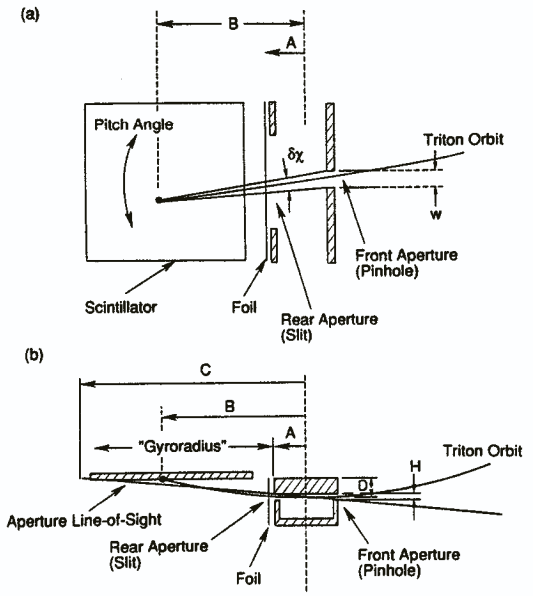

FIG. 2. Details of the detector, showing the geometry for measuring (a) pitch angle and (b) gyroradius or energy. The pitch angle is determined by the angle between the particle impact position and the front pinhole, with a geometrical angular resolution set by the front aperture width. The energy is determined from the impact position B with a resolution set by the aperture height H (full height). For the present detector, A ≈ 0.5 cm, B ≈ 2 cm, C ≈ 4 cm, D ≈ 0.4 cm, H ≈ 0.1 cm and W ≈ 0.2 cm. The design also ensures that the direct line of sight through the apertures misses the scintillator at C.

made as large as possible, consistent with the desired pitch angle and energy resolution.

Other features of the design are that the vertical distance, D = 0.4 cm, between the aperture centre and the scintillator is minimized in order to avoid overheating of the top of the box due to plasma flow (given this aperture location) and that the size of the detector box is constrained by the vacuum port to approximately 2 in × 2 in. The direct line of sight through the aperture pair is also constrained so as not to intersect the scintillator itself in order to avoid a soft X-ray background [5], setting an upper limit on the aperture height. Note also that the effect of the 3 μm aluminium foil behind the slit (used to block plasma light) is taken into account in evaluating the incident particle energy.

The ultimate time resolution of this system is determined by the decay time of the ZnS(Ag) scintillation process, which is less than 10 μs [5]. However, for the present experiment the time resolution is set by the video camera framing rate of 16 ms per field, which is still short compared to TFTR time-scales of ≈1 s.

The detector shown in Fig. 1 is mounted on a bellows assembly and inserted vertically from below into the TFTR vessel at R = 265 cm, i.e. very near the vessel major radius. The radial location of the top of the box is chosen to be r = 101.5 cm, i.e. well outside the typical plasma radius of a = 80 cm. At this location the apertures are just inside the radius of the local obstacles at the vessel wall, such that the escaping orbits are not obstructed on their way towards the detector. At this location the temperature inside the detector box during TFTR operation (as measured with a thermocouple) is always less than 90°C.

The sensitivity of the system to particle flux at the scintillator was calibrated before installation using an ^{241}Am alpha source. For an expected flux of $\approx 10^8$ tritons·cm^{-2}·s^{-1} at the scintillator it was necessary to use an intensified video camera, partly because of the factor-of-ten light attenuation through the ≈7 m plastic fibre bundle. The sensitivity of the system is adjustable by varying the gating time per field of the camera's microchannel plate.

Note that an estimate of the particle flux to the scintillator needs to include both the 1 MeV tritons and a 30–40% contribution from 3 MeV protons, since these two particles have identical gyroradii and orbits in the plasma and are measured together on the scintillator (the 0.8 MeV ^{3}He particle does not pass through the 3 μm foil). For simplicity, in the following I will often refer to 'triton' detection but will mean triton and proton detection.

The primary experimental difficulty with this prototype detector was a large unexpected background proportional to the soft X-ray flux emitted from the plasma. This turned out to be due to the 20–40 keV X-ray tail of the thermal plasma centre ($T_e(0) \approx$ 5–7 keV) penetrating the top of the carbon box and the quartz scintillator substrate. This background resulted in a maximum signal-to-background ratio of only about 4 and prevented triton detection above about 1.3 MA.

However, since the location of the soft X-ray source was relatively far from the detector, it produced a reproducible 2-D pattern on the scintillator which could be substracted out fairly easily by using a reference video field from an Ohmic shot which had large soft X-ray emission but no triton creation. This background signal pattern was normalized at a point on the scintillator not expected to be hit by tritons, either at very low pitch angles or at high gyroradius (the standard soft X-ray monitor could not be used for normalization because its spectral sensitivity was different from that of the scintillators). There was also

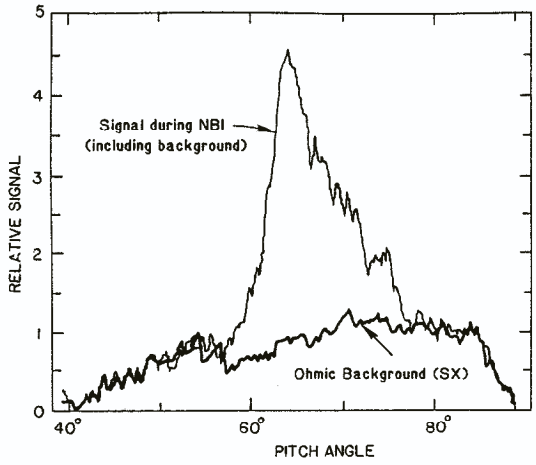

FIG. 3. Example of the scintillator light intensity versus pitch angle as measured at a gyroradius corresponding to 1 MeV tritons (or 3 MeV protons). The signal curve is taken from one video frame exposed for 0.5 ms at a neutron (triton) source rate of 5×10^{15} n·s^{-1}. The background curve is obtained from an Ohmic discharge when the neutron rate is negligible but the soft X-ray flux is high. The difference between these two curves represents the net triton signal.

a small background proportional to the neutron/gamma flux, which was automatically subtracted out in this process.

Another practical difficulty in these measurements was the variation in the optical sensitivity across the scintillator which was due to vignetting and to the imperfect plastic fibre bundle which carried the 2-D image to the camera. This was corrected for by assuming that the soft X-ray background flux onto the scintillator was uniform (as is plausible, since the box was directly below the plasma centre) and by using the shape of the background curve as an indication of the relative optical sensitivity.

The detector was removed after about four months in TFTR and recalibrated. The optics and foil were intact and the scintillator calibration was unchanged. The only damage to the probe was some minor surface erosion of the carbon armour which was in contact with the plasma flow.

3. EXPERIMENTAL RESULTS

The 2-D images of the scintillator light emission were stored on video tape and later digitized. The results were compared with the classical first-orbit prompt loss model.

3.1. Pitch angle dependence

Figure 3 shows an example of the light intensity versus pitch angle as measured across the scintillator. In this case the TFTR plasma current I was 0.9 MA, the toroidal field B_T was 48 kG, the neutral beam injection (NBI) power was 12 MW, and the data were taken from a single video field exposed for 0.5 ms when the neutron rate S was 5×10^{15} n·s^{-1}. This signal was evaluated at the 'gyroradius' co-ordinate corresponding to 1 MeV tritons, averaged over $\approx \pm 0.4$ cm on the scintillator. The signal in this (and all other) cases had a peak at $\chi \approx 60$–$65°$ with respect to the magnetic field, as measured from the plasma current direction.

Also shown in Fig. 3 is a soft X-ray 'background' curve which was measured similarly during a 1.4 MA Ohmic discharge when there was a large soft X-ray background but no significant triton production. This background curve represents the response of the system to X-rays penetrating the top of the detector box. The background level during NBI shots was obtained by normalizing this 'Ohmic background' curve to the 'triton signal' curve at $\chi \approx 50°$ (or $\chi \approx 80°$) where no triton loss is expected. Thus, only the *difference* between the two curves in Fig. 3 represents the net escaping triton flux.

The net triton signal from Fig. 3 is plotted versus pitch angle in Fig. 4. For this figure an additional correction was made to account for the variation in optical sensitivity of the system between $\chi \approx 45°$ and $\chi \approx 85°$ (which is the range of the scintillator image), as taken from the shape of the Ohmic background curve (e.g. correcting for a defect in the fibre bundle at $\chi \approx 58°$). The width of this experimental curve includes a ± 4–$5°$ instrumental broadening due to the finite aperture width W(± 2–$3°$), the relay lens optics ($\pm 2°$) and the fibre bundle ($\pm 2°$). The alignment in pitch angle is accurate to about $\pm 3°$, as shown by the horizontal error bar.

The triton flux versus pitch angle expected from the prompt-loss model for this discharge was calculated using a standard particle orbit code [6, 7], the results of which are also shown in Fig. 4. The flux was expected to be peaked at $\chi \approx 60$–$65°$ for 1 MeV tritons (or 3 MeV protons), as in previous calculations of escaping alpha flux [1, 8, 9]. This corresponds to the pitch angle of the 'fattest banana' orbit which passes closest to the high triton source region at the plasma centre, as shown in Fig. 5(a). Note that the 'first-orbit model' curve in Fig. 4 represents the range of expected results over an assumed triton source

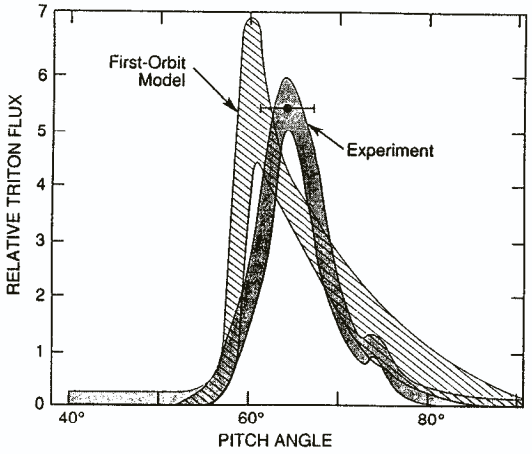

FIG. 4. Measured and predicted (first-orbit loss model) flux versus pitch angle for 1 MeV tritons. The experimental curve is obtained from Fig. 2 after background subtraction and optical sensitivity correction. The model curve comes from the particle orbit code and represents the range of plausible radial source and current profiles. The two curves agree to within the joint uncertainties, including an ≈3° angular alignment uncertainty shown by the error bar. Note that only the relative shapes of the flux versus pitch angle are plotted here (the absolute flux comparison is discussed in Section 3.5).

profile, $S(r) \propto [1 - (r/a)^2]^{4-8}$, and an assumed plasma current distribution, $J(r) \propto [1 - (r/a)^2]^{3-5}$, where a narrower profile corresponds to a narrower pitch angle distribution.

The conclusion from Fig. 4 is that the measured pitch angle distribution of the escaping 1 MeV tritons is approximately consistent with the expected first-orbit loss, at least to within the pitch angle resolution and alignment uncertainties in this experiment. This is the first time-resolved experimental measurement of such a pitch angle distribution of escaping fusion products from a tokamak.

3.2. Energy dependence

Figure 6 shows two examples of the light intensity versus the 'gyroradius' co-ordinate as measured across the scintillator (this co-ordinate is approximately proportional to $\rho^{1/2}$). Each of these curves is taken from one video frame during the steady state of a 0.9 MA NBI discharge; case (a) at B_T = 48 kG is similar to the shot in Fig. 2, while case (b) at B_T = 28 kG has a lower toroidal field. For both cases the signal is evaluated in the pitch angle range $\chi \approx 60$–$65°$ where the triton signal is maximum.

The location of the peak of this signal along the gyroradius co-ordinate in Fig. 6 and movement of this peak with B_T are approximately consistent with the detection of full-energy ≈1 MeV tritons. The expected locations, shown by the vertical bars, are calculated assuming that the gyroradius is proportional to $\sin \chi/B_T$ and take into account the 25% energy loss of tritons in the aluminium foil and the slightly larger gyroradius of 3 MeV protons orbits (due to relatively lower energy loss in the foil).

The broadness of these peaks, about ±0.8 cm FWHM for the 48 kG case (at the scintillator), is close to that expected from the finite aperture height, which allows a single gyroradius spread of $\delta B \approx (\rho/A)H/2 \approx \pm 0.6$ cm in this direction (see Fig. 2(b)). Additional broadening is due to the triton/proton gyroradius difference (after the foil), to the optical and fibre bundle resolutions and to the ≈25% Doppler width of 1 MeV tritons.

The conclusion is that the measured triton energy of ≈1 MeV (±50%) is approximately consistent with the first-orbit loss model, which predicts that a negligible energy loss should before the tritons escape. Although the energy distribution of escaping fusion products has been measured more accurately with surface barrier detectors [10]. This observed variation of the gyroradius with B_T confirms the basic triton detection mechanism of this device.

3.3. Time dependence

Figure 7 shows an example of the time dependence of the escaping triton signal, again for a 0.9 MA shot similar to that in Figs 2 and 3, with NBI between

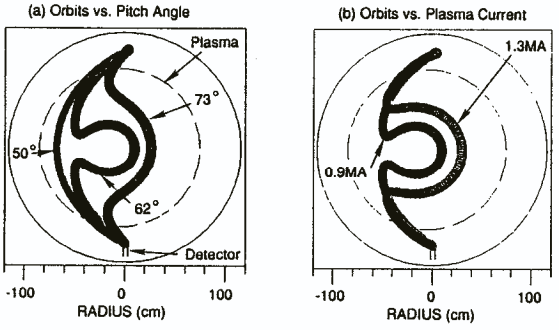

FIG. 5. Orbit code results showing typical 1 MeV triton trajectories expected for different pitch angles (a) and plasma currents (b). All orbits are constrained to go through the detector. In (a) the plasma current is 0.9 MA and in (b) the pitch angle is 62°.

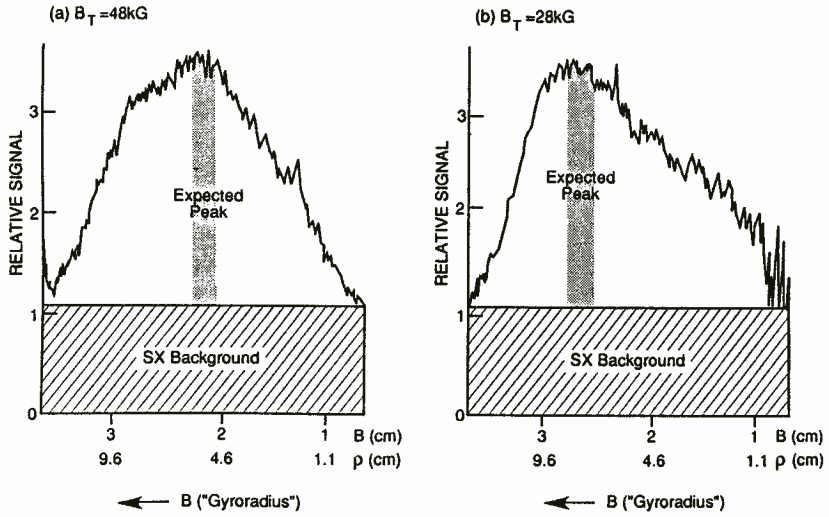

FIG. 6. Example of data for light intensity versus the 'gyroradius' co-ordinate as measured at a pitch angle $\chi \approx 60$–$65°$ for two different toroidal fields. The 'gyroradius' co-ordinate B is approximately proportional to $\rho^{1/2}$, as shown in Fig. 2. In both cases the peak signal lies near the position on the scintillator expected for 1 MeV tritons (right edge of shaded region) or 3 MeV protons (left edge of shaded region). The expected shift in the peak due to $\rho \propto B_T^{-1}$ is observed. The large width of these curves is due to the finite aperture height, approximately as expected.

4 and 5 s. In this case the triton signal is measured within an area near the peak of the 2-D distribution on the scintillator ($\chi \approx 60$–$65°$ and E $\approx$ 1 MeV), and the time-dependent background is subtracted out by using an area of the scintillator away from possible triton impact (i.e. $\rho \approx 10$ cm).

The escaping triton flux follows the global triton source rate fairly closely in time, as can be seen by comparing the escaping triton flux with the global neutron (= triton) source rate in Fig. 7. The major uncertainty in this comparison, as indicated by the error bars, comes from subtracting out the soft X-ray background, particularly after NBI when the soft X-ray background is still high while the triton rate is falling. There is also an ≈ 10 ms uncertainty of the camera triggering time with respect to the TFTR neutron signal in this system. Note also that some differences between the global source and the escaping triton flux are expected because of possible time-dependent changes in the radial profiles of the triton source and the plasma current.

The tentative conclusion is that the measured time dependence of the escaping triton flux is approximately consistent with the behaviour expected for 'prompt' first-orbit loss, in which the escaping triton flux should follow the triton source within < 100 μs. Particularly interesting is the apparent absence of non-prompt loss during the period 0.2–0.5 s after NBI when the confined triton population should be high (since the classical triton slowing-down time is ≈ 1 s). The expected non-prompt loss at high energy (>0.5 MeV) due to pitch angle scattering is typically $\ll 10\%$ of the prompt loss [11], consistent with this observation.

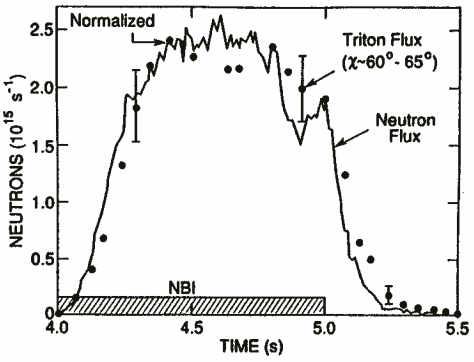

FIG. 7. Measured time dependence of the triton signal evaluated at a pitch angle $\chi \approx 60$–$65°$ and a triton energy E ≈ 1 MeV. The escaping triton signal roughly follows the triton source rate as monitored by the 2.5 MeV neutron flux, as is expected from the prompt first-orbit loss model. Note that there is a slight detector saturation at the peak of the triton signal which causes those points to be somewhat low.

3.4. Plasma current dependence

Figure 8 shows some examples of the light intensity versus pitch angle similar to those of Fig. 2, but for plasma currents in the range 0.9–1.3 MA. Each curve was taken from a single video field at a time during NBI when the neutron rates were identical to within ±10% (at $S = 5 \times 10^{15}$ n·s^{-1}). All shots were taken on the same day at $B_T = 48$ kG with 12 MW of NBI. The shape of the background curve is the same for each case and was normalized to the triton signal at $\chi \approx 50°$ as described in Section 3.1.

These examples show that the escaping triton flux (per neutron) decreases as the plasma current increases. This trend is plotted for about twenty such shots in Fig. 9, where the escaping triton flux is evaluated at the peak in pitch angle ($\chi \approx 60$–$65°$). Note that the soft X-ray background increases with plasma current as the triton signal is decreasing, such that the triton signal is hardly distinguishable above the background at 1.3 MA.

The expected first-orbit loss versus plasma current at this pitch angle is also shown in Fig. 9. At higher currents the expected flux is lower because the orbits originate nearer the plasma edge, as shown in Fig. 5(b). The shaded area in Fig. 9 represents the range of variation due to uncertainty in the triton source rate (parabolic exponent 4–8) and the current profile (parabolic exponent 3–5), with the more peaked profiles having a more rapid fall-off with plasma current. The approximate invariance of the shape of the pitch angle distribution seen in Fig. 8 is also predicted in the orbit code.

The conclusion is that the measured plasma current dependence of the escaping triton flux is also roughly consistent with the expected variation of first-orbit losses, at least to within the joint uncertainties of the experiment and the model. This is the first experimental measurement of the current dependence of escaping fusion products in a tokamak.

3.5. Absolute flux

Up to this point, only the *relative* pitch angle, energy, time and current dependences of the escaping triton flux were discussed. The absolute triton flux

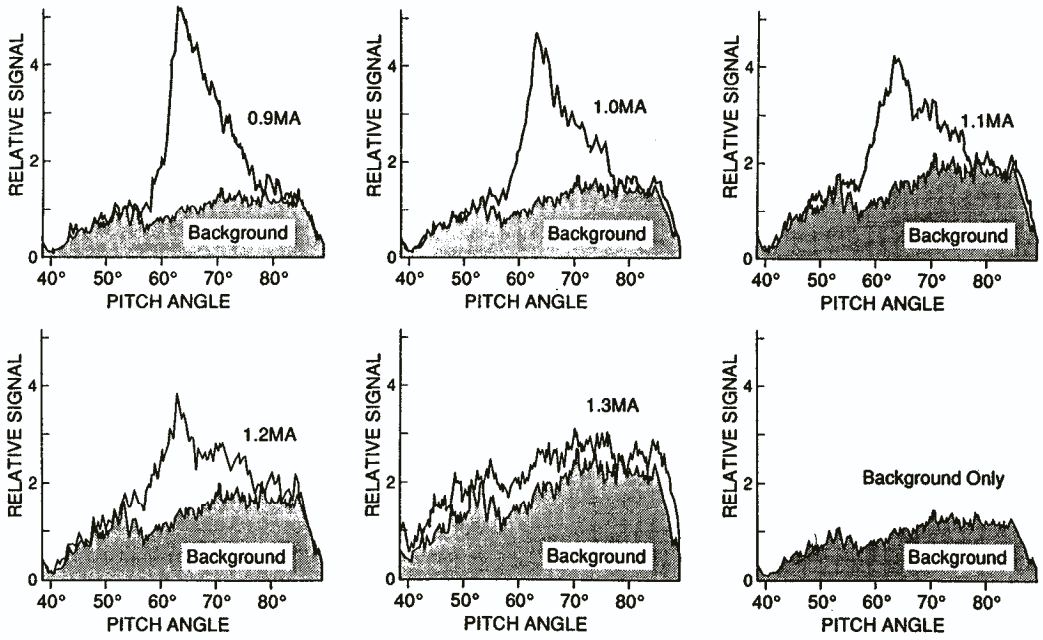

FIG. 8. Examples of the measured light intensity versus pitch angle similar to Fig. 2, but for plasma currents in the range 0.9–1.3 MA. These signals are all taken at a neutron rate of 5×10^{15} n·s^{-1} and a gyroradius corresponding to 1 MeV tritons. The net triton signal decreases as the plasma current increases, until at 1.3 MA the triton signal is hardly observable above the soft X-ray noise level (which increases with plasma current). The shape of the background curve is taken from a 1.4 MA Ohmic discharge with no escaping tritons.

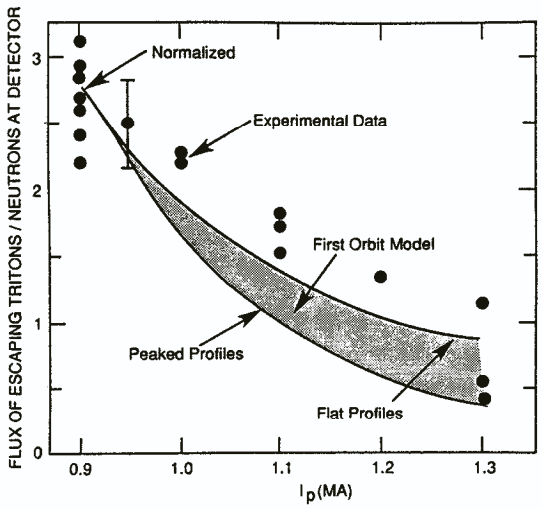

FIG. 9. Escaping triton flux per neutron versus plasma current, evaluated at a pitch angle $\chi \approx 60$–$65°$ and a triton energy $E \approx 1$ MeV. The experimental points come from a series of shots such as those shown in Fig. 8 (after background subtraction). The shaded first-orbit model region represents the same range of profile assumptions as used for Fig. 4. The measured decrease in escaping triton flux with increased plasma current is roughly consistent with the model. The error bar indicates approximate shot-to-shot variation.

can be estimated from a bench-top calibration of the system with an ^{241}Am alpha source, made with the scintillator plate reversed.

For this estimate, an assumption concerning the relative scintillation light intensity for ^{241}Am alphas (4.5 MeV after source attenuation) versus tritons and protons has to be made, since no D–D triton source was available for calibration. As discussed previously [5], if the light emission is assumed to be proportional to the energy deposited in the scintillator, then the 4.5 MeV alpha produces about four times the light of a 1 MeV triton, and the 3 MeV proton produces about 30% the light of a 1 MeV triton, taking into account the attenuation in the foil and the penetration distance through the thin ZnS layer. With this assumption, the total triton flux at the scintillator for the 0.9 MA case of Fig. 2 (obtained by integrating over an impact area of $\approx 0.6 \times 1.6$ cm) is $\approx 2 \times 10^8$ tritons$\cdot$s^{-1} at a neutron flux of 3×10^{15} n$\cdot$s^{-1}. This estimate of triton flux is uncertain by at least a factor of two to three, because of the assumed scintillator response to protons and tritons, the uncertainties in the ^{241}Am calibration itself and the difficulty of integrating the measured triton flux over the scintillator area in the presence of the large soft X-ray background.

The theoretically expected triton flux incident on the scintillator for this case was calculated using the orbit code [6, 7], which models the prompt-loss flux through a pair of apertures similar to those in this experiment. The result for a 0.9 MA case was $\approx 3 \times 10^8$ tritons$\cdot$s^{-1} at an assumed neutron rate of 3×10^{15} n$\cdot$s^{-1}, with about a factor of two variation due to the range of possible source and current profiles. With the additional uncertainties in the neutron source calibration and in the aperture modelling, the net result is uncertain by at least a factor of three.

Therefore, the tentative result is that the absolute flux of escaping tritons is approximately consistent with the predicted first-orbit loss, but only to within the large joint uncertainties. This also appears to be consistent with the classical (to within a factor of two) triton burnup measured in TFTR [12] and JET [13].

4. CONCLUSIONS

The first results from a new triton imaging detector in TFTR, concerning the pitch angle, energy and time dependence of escaping tritons, have been reported. These results are consistent in many respects with the expected classical first-orbit loss model. In particular, the predicted peak in the flux versus pitch angle (Fig. 4) and the decrease in escaping flux with increased plasma current (Fig. 9) have been measured clearly in tokamaks for the first time. The apparent absence of non-prompt loss is also seen in the time dependence of the triton signal, particularly after NBI (Fig. 7).

The prototype detector system described in Section 2 has worked succesfully, but could be improved at several points. Most important would be an improvement in soft X-ray shielding above the scintillator, which would eliminate the largest background and so permit a better measurement of the high frequency components of the signal (3 mm of stainless steel shielding will be used in future detectors). Also planned is the replacement of the plastic coherent fibre bundle by lower-loss, radiation resistant quartz fibres.

Although the present results are consistent with the trends predicted by the simple prompt-loss model, it is difficult at this point to exclude the possible influence of toroidal field (or MHD induced) ripple [14, 15], since these effects tend to produce the same relative trends as the prompt-loss model. For example, stochastic diffusion in the toroidal field ripple tends to broaden the effective triton source profile on a relatively fast time-scale ($\ll 100$ ms) and so it would be difficult

to distinguish from first-orbit loss with a broader radial profile, at least without an accurate absolute calibration. Future experiments might try to change the effective ripple to resolve this effect, for example through radial plasma movement. Also useful in this regard would be a poloidal/toroidal array of detectors, since the stochastic ripple losses tend to occur closer to the outer equator than prompt losses.

The detector described here can also be used with D–T generated escaping 3.5 MeV alpha particles, which have nearly the same gyroradius as 1 MeV tritons or 3 MeV protons. For D–T alphas the dominant background should be the relatively small neutron or gamma interactions with the scintillator itself [5]; if this were the case, then the ≈ 100 times larger signal level should allow reduced apertures and improved energy and/or pitch angle resolution.

ACKNOWLEDGEMENTS

Particular thanks go to J.D. Strachan and K.M. Young for encouraging and supporting this project, and to T. Deverell for help with its construction. Thanks are also due to F. Dylla, K. Hill, D. Johnson, L. Johnson, P. LaMarche, D. Manos, K. Owens and M. Ulrickson of PPPL for advice on the detector design.

This work was supported by the Unites States Department of Energy, under Contract No. DE-AE02-76-CHO3073.

REFERENCES

[1] KOLESNICHENKO, Yu.I., Nucl. Fusion **20** (1980) 727.
[2] ZWEBEN, S.J., FURTH, H.P., MIKKELSEN, D.R., REDI, M.H., STRACHAN, J.D., Nucl. Fusion **28** (1988) 2230.
[3] ZWEBEN, S.J., Phys. Scr. **T16** (1987) 119.
[4] MURPHY, T.J., STRACHAN, J.D., Nucl. Fusion **25** (1985) 383.
[5] ZWEBEN, S.J., Rev. Sci. Instrum. **60** (1988) 576.
[6] CHRIEN, R.E., STRACHAN, J.D., Phys. Fluids **26** (1983) 1953.
[7] HEIDBRINK, W.W., STRACHAN, J.D., Rev. Sci. Instrum. **56** (1985) 501.
[8] HIVELY, L.M., MILEY, G.H., Nucl. Fusion **17** (1977) 1031.
[9] BAUER, W., WILSON, K.L., BISSON, C.L., GOLDSTON, R.J., Nucl. Fusion **19** (1979) 93.
[10] BOSCH, H.-S., SCHUMACHER, U., ASDEX Team, in Controlled Fusion and Plasma Heating (Proc. 13th Eur. Conf. Schliersee, 1986), Vol. 10C, Part II, European Physical Society (1986) 1.
[11] ANDERSON, D., BATISTONI, P., Nucl. Fusion **28** (1988) 2151.
[12] BARNES, C.W., BOSCH, H.S., NIESCHMIDT, E., et al., in Controlled Fusion and Plasma Heating (Proc. 15th Eur. Conf. Dubrovnik, 1988), Vol. 12B, Part I, European Physical Society (1988) 87.
[13] CONROY, S., JARVIS, O.N., SADLER, G., HUXTABLE, G.B., Nucl. Fusion **28** (1988) 2127.
[14] TANI, K., TAKIZUKA, T., AZUMI, M., KISHIMOTO, H., Nucl. Fusion **23** (1983) 657.
[15] WHITE, R.B., MYNICK, H.E., Alpha Particle Confinement in Tokamaks, Rep. PPPL-2563, Princeton Plasma Physics Laboratory, Princeton, NJ (1988).

(Manuscript received 16 December 1988
Final manuscript received 3 March 1989)